JOURNAL OF MATERIALS SCIENCE **39** (2004) 2827–2833

# Initiation and propagation behaviors of interior microflaws in the pyrolysis of an air-cured polycarbosilane precursor fiber

ZENG-YONG CHU, CHUN-XIANG FENG, YONG-CAI SONG, YING-DE WANG, JUN WANG, XIAO-DONG LI, JIA-YU XIAO
*Key Lab of New Ceramic Fibers and Composites, School of Aerospace and Materials Engineering, National University of Defense Technology, Changsha 410073, People's Republic of China*
*E-mail: Z.Y.Chu@163.net*

In the preparation of Nicalon-type Si–C–O fibers using a normal-pressure synthesized polycarbosilane precursor, a network of microflaws were detected on the cross-section of ceramic fibers obtained. Cross-section morphologies of the interior microflaws were investigated via SEM technique after certain temperature pyrolysis and their initiation and propagation behaviors were studied accordingly. The results showed that no microflaws came into being at the temperature up to 600°C due to the organic nature of the material. As a result of high weight loss and composition change, however, microflaws initiated over 600°C, formed at ~700°C and propagated along the "core-edge" direction from 700–900°C. Up to 1100°C, a microflaw network was formed because new microflaws generated across the oriented ones and interconnected them to form a network. 

## 1. Introduction

Based on the successful exploring work of Yajima *et al*. [1], there has been much recent interest in the preparation of ceramic materials, especially fibers, by the pyrolysis of polymer precursors as the process offers many new advantages such as a lower synthesis temperature and an adjustable composition at atomic level [2–6]. Up to now, various ceramic fibers, such as Nicalon, Tyranno and HPZ, have become commercially available [5]. However, the fibers with Si–C–O, Si–Ti–C–O and Si–N–C–O compositions generally have densities lower than those calculated from a volume additivity rule, implying the presence of voids (even up to 25%) [7, 8]. Small angle X-ray scattering (SAXS) techniques also confirmed the presence of closed, globular nanopores, with little or no open porosity detected on the surface from BET surface analysis [8–10]. This is explained by the formation of nanochannels in the early stages of the pyrolysis process during loss of large volumes of pyrolysis gases and nanopores are formed in the later stages by viscous collapse of nanochannels accompanying ceramic densification [8]. In addition, little or no micrometer-scale flaws (pores) were detected and reported, which, as known, are probably due to a relatively dense structure that is responsible for the high strength of such fibers [11].

However, using a normal-pressure synthesized polycarbosilane (PCS) instead of the PC-470 type PCS obtained with an autoclave [1, 11], a network of microflaws was detected on the cross-section of the Si–C–O fibers, whose largest size is even as high as 1 $\mu$m [12]. This kind of microflaw must behave much more differently than nanochannels or nanopores. To know how the microflaws initiate and propagate is important to improve mechanical properties, although the tensile strength has reached an acceptable level (~2.90 GPa for an average diameter of 9 $\mu$m).

However, it is impossible to *in situ* observe the initiation and propagation behaviors via the SEM technique since the pyrolysis temperature is as high as 1250°C. As an alteration, the air-cured precursor fibers were fired up to certain temperatures firstly and then cooled down to room temperature to be observed. Also because of difficulties in repyrolysis of the single fiber, different filaments were studied for each condition, with typical ones selected to conclude the initiation and propagation behaviors. At the same time, chemical composition, density, weight loss and longitudinal shrinkage were also recorded as necessary information to interpret the corresponding phenomena.

## 2. Experimental procedure

A PCS precursor was synthesized from polydimethylsilane (PDMS) at normal pressure up to 450°C for 6 h [13]. The PCS was filtered to remove impurities and then distilled at 300°C under 100 mmHg to vaporize low molecular weight fractions. The spinnable PCS obtained has a softening point of 202 ± 3°C and a molecular weight of 1523 Da with a dispersion coefficient of

TABLE I Characteristics of the air-cured PCS precursor fibers

| Sample | Gel content (%) | Weight gain (%) | Reaction degree of Si–H bond (%) | Filaments/ yarn |
|---|---|---|---|---|
| Air-cured PCS | 100 | 11.2 | 85 | 200 |

1.8. The PCS was heated to 300°C in a container under a nitrogen atmosphere and was extruded out through a multihole spinneret [14]. Then, the continuous green fibers were transported to a curing oven and heated slowly, 15°C/h, up to 190°C for 4 h in air. After that, the air-cured PCS fibers, as characterized in Table I, were cut into 20 cm long and heated in a quartz tube under inert atmosphere, up to certain temperature with a holding time of 1 h.

Curing degree and heating rate play an important role in determining the ceramic yield and density, and in turn, have a great influence on the interior microflaws of the fibers. An oxidation process up to 190°C with a holding time of 4 h was selected for the curing of PCS fibers because the highest tensile strength could be obtained in this case, as reported previously [15]. Moreover, slow heating rates are preferred in the preparation of polymer-derived ceramics [2] and so, a relatively slower one, 100°C/h, was adopted in this study.

Thermal gravimetric analysis (TGA) was conducted using a NETZSCH STA 449C (USA) instrument with a high purity nitrogen flow (2 ml/min) as the protecting atmosphere. The heating rate was also 100°C/h so as to simulate the pyrolysis process. Longitudinal shrinkage was recorded through a load cell and a scale ruler out of the quartz tube. The load cell was connected with PCS fibers through a carbon bundle.

For the air-cured fibers and their pyrolyzed products, fourier transform infrared spectroscopy (FT-IR) was obtained over the range of 4000 to 400 $cm^{-1}$ using a Perkin Elmer System 2000 spectrometer. KBr discs were used, prepared by compressing a finely ground mixture of about 3 mg of the sample and 200 mg of KBr powder.

The sink-float method was used to measure fiber densities, following a simplified ASTM C729-75 standard test. Solutions with densities of 2.30 to 3.20 $g/cm^3$ were prepared by mixing $\alpha$-bromonaphthalene ($C_{10}H_7Br$) and sym-tetrabromoethane ($Br_2CHCHBr_2$) at room temperature with increments of 0.05 $g/cm^3$.

Elemental chemical analysis was performed for silicon, carbon, oxygen and hydrogen. C and H content were determined by a thermal combustion method. About 1 mg of PCS was placed in a container and heated under oxygen in a combustion tube to 1800°C. The amounts of carbon and hydrogen were measured as $CO_2$ and $H_2O$ respectively by gas chromatography. For Si determination, about 20 mg of sample was fused in a mixture of KOH and $KNO_3$ in a nickel crucible at 650°C to release Si as a silicate that was then detected by atomic absorption. Oxygen was determined using a TC-436 N/O analysis instrument from LECO Inc. (USA).

Scanning electron microscopy (SEM) was used to measure fiber diameters and to examine fiber microstructure, i.e., the cross-section morphology. Experiments were conducted on a Jeol JSM-6300 microscope, Japan. SEM samples were prepared by tensile breaking fibers in oil, dissolving them in ethanol and mounting them on the edge of an aluminum stub using double stick tape with fracture surface facing up. Samples were sputter coated with a layer of Au to enhance their conductivity before observation.

## 3. Results

### 3.1. SEM characterization

Cross-section morphologies of the air-cured PCS fibers heated up to certain temperature are shown in Fig. 1, and their corresponding properties are shown in Table II. Note that all the photos obtained in the paper are using a uniform magnification, ×30 K.

For the as-spun, as-cured and as-pyrolyzed fibers below 600°C, all showed a similar morphology to that of Fig. 1a, that is, no microflaws could be detected at the uniform magnification (×30 K). However, this is not the case for a 700°C-pyrolyzed fiber, as shown in Fig. 1b: microflaws appeared with the largest flaw size approaching 0.2 $\mu$m.

Fig. 1c is a photo of the 800°C-pyrolyzed fiber, which exhibits a rough morphology with a large inclusion at the center. As being extensively studied, the inclusion is mainly introduced during the preparation of PCS as partly pyrolyzed products due to local thermal accumulation [13] and in general, PCS should be strictly filtered to remove impurities prior to spinning [14]. Interestingly, however, there seems existing a propagating direction for the flaws from the core to the surface and this phenomenon is more evident in Fig. 1d and e, which are the photos of PCS fibers pyrolyzed

TABLE II Characteristics of the air-cured polycarbosilane fibers with increase of heat-treatment temperature

| Characteristics | #0 | #1 | #2 | #3 | #4 | #5 | #6 | #7 | #8 | #9 | #10 |
|---|---|---|---|---|---|---|---|---|---|---|---|
| Heat treat. temp. (°C) | RT | 400 | 500 | 600 | 700 | 800 | 900 | 1000 | 1100 | 1200 | 1250 |
| Weight residue (wt%) | 100 | 100 | 94.2 | 89.2 | 87.7 | 84.4 | 81.9 | 81.7 | 81.1 | 81.0 | 80.8 |
| Density ($g/cm^3$) | 1.10 | 1.12 | 1.18 | 1.22 | 1.55 | 2.01 | 2.30 | 2.34 | 2.38 | 2.40 | 2.40 |
| Composition (wt%) | | | | | | | | | | | |
| Si | 47.31 | 47.38 | 48.14 | 48.28 | 49.87 | 51.36 | 51.72 | 53.04 | 53.96 | 54.02 | 53.98 |
| C | 33.70 | 33.75 | 32.72 | 32.54 | 32.06 | 31.05 | 30.57 | 30.48 | 30.35 | 30.15 | 30.07 |
| O | 13.16 | 12.94 | 13.21 | 13.37 | 14.34 | 15.63 | 16.72 | 16.21 | 16.22 | 16.18 | 16.11 |
| H | 6.24 | 6.18 | 5.95 | 4.68 | 3.09 | 1.87 | 0.80 | 0.33 | 0.14 | 0.08 | 0.05 |

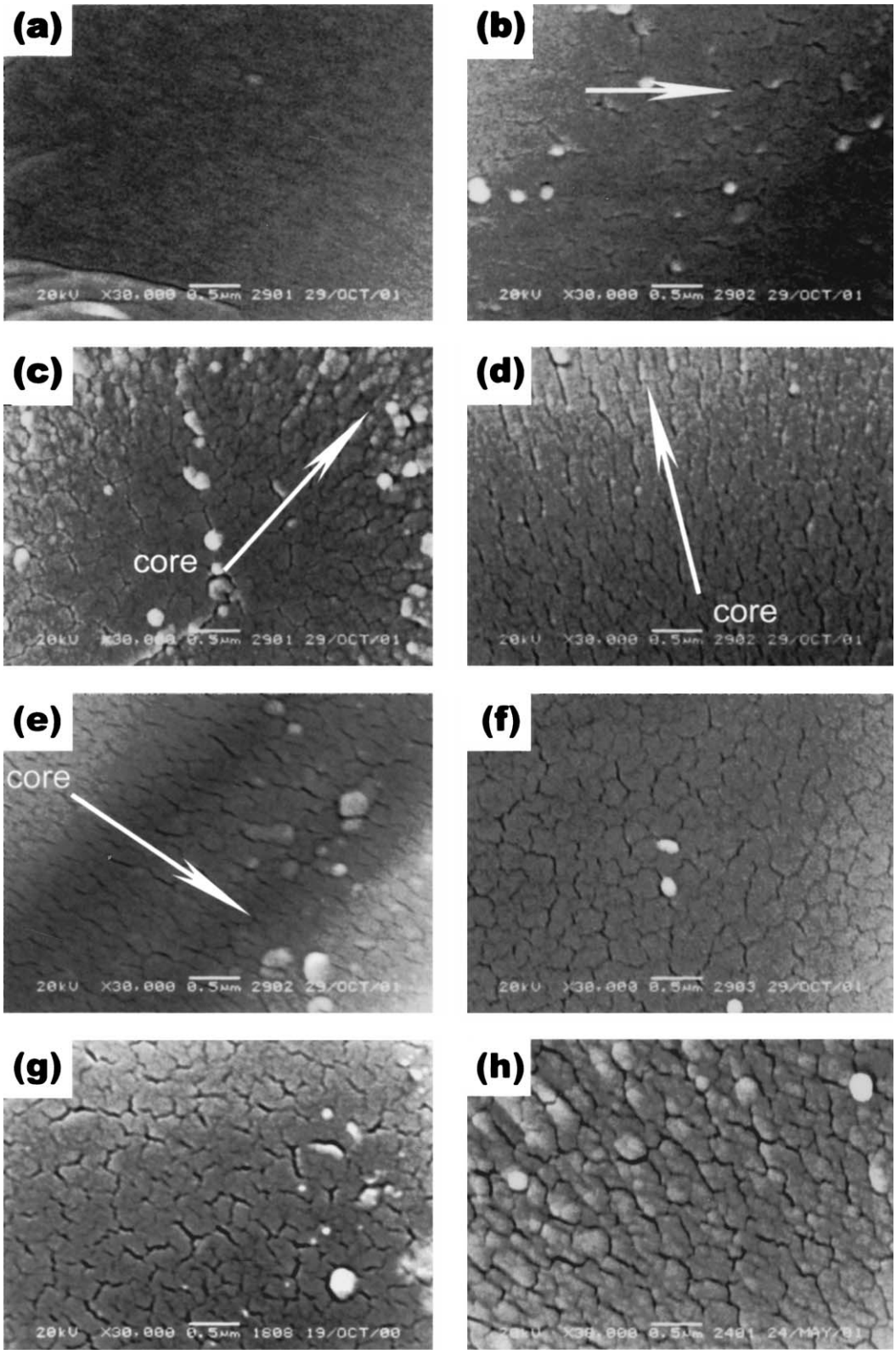


*Figure 1* Cross-section morphologies (×30 K) of the air-cured PCS fibers heated up to 600°C (a), 700°C (b), 800°C (c), 900°C (d), 1000°C (e), 1100°C (f), 1200°C (g) and 1250°C (h), all of a 1 h-maintenance at the highest temperature.

up to 900 and 1000°C respectively. Furthermore, the largest microflaws have propagated to sizes approaching 1.0 $\mu$m. But when the pyrolysis temperature rises higher, the preferred orientation seems to have disappeared and the microflaws were interconnected into a network form, as shown in Fig. 1f–h for the fibers pyrolyzed up to 1100, 1200 and 1250°C, respectively. In addition, the area fraction of the microflaws was also increased.

### 3.2. FT-IR characterization

The wave numbers corresponding to the various absorption bands in the FT-IR spectra of the as- spun, as-cured and as-pyrolyzed PCS fibers (Fig. 2) are given in Table III. These assignments were based on the reported data for PCS and the general features in the spectrum of this normal pressure synthesized PCS (Fig. 2a) appear similar to the published spectrum of the PC-470 type PCS [1, 11, 16–19].

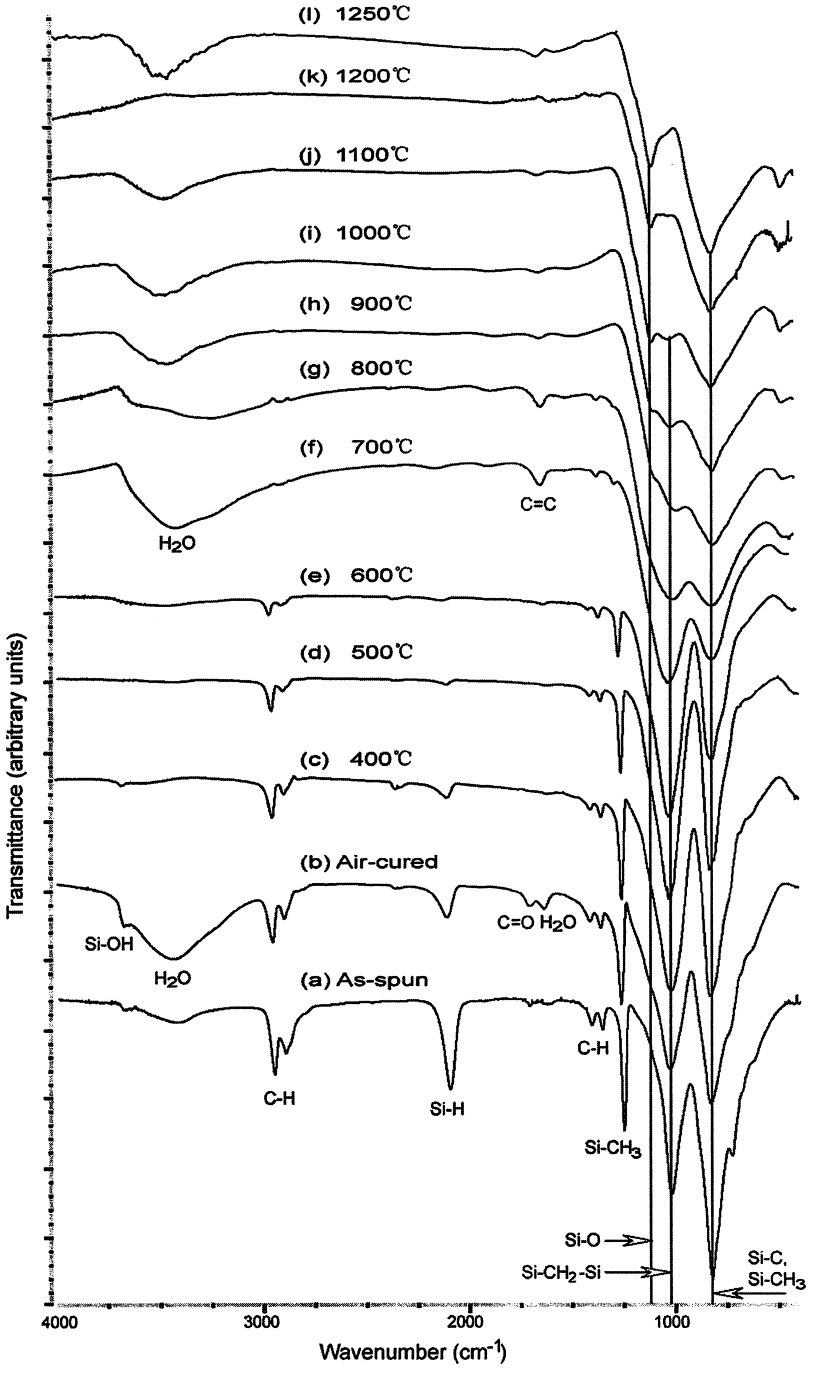


*Figure 2* FT-IR spectra of the air-cured PCS fibers heated up to certain temperature with a maintenance of 1 h.

For the as-spun PCS fibers in Fig. 2a, FT-IR indicates that the major bonds present were Si–$CH_3$ (1250 $cm^{-1}$) and Si–H (2100 $cm^{-1}$). The broad band at around 1020 $cm^{-1}$ was due to the overlap of the bands due to $CH_2$ groups in Si–$CH_2$–Si units (1020 $cm^{-1}$) and a band due to Si–O bonds (1080 $cm^{-1}$). The small band at around 3700 $cm^{-1}$ could have been due to O–H stretching of Si–OH [17] or water. Si–C (820 $cm^{-1}$) and Si–H (880 $cm^{-1}$) bonds could have contributed to the broad band around 800 $cm^{-1}$ [16].

After air curing, as shown in Fig. 2b, the absorption peaks due to Si–H, C–H and Si–$CH_3$ groups decreased in intensity on curing, particularly the Si–H and C–H bonds of Si–$CH_3$ groups. An absorption band at 1710 $cm^{-1}$ due to C=O stretching, as well as the O–H stretching band in Si–OH groups (3700 $cm^{-1}$), the stretching vibration band of adsorbed water at around 3500 $cm^{-1}$ and a deformation band of $H_2O$ at 1620 $cm^{-1}$ were observed. In addition, a broad band at around 1080 $cm^{-1}$ superimposed on the band around 1020 $cm^{-1}$ was assigned to Si–O stretching in Si–O–Si and Si–O–C units. The whole phenomena resulted from the oxidation of Si–H group by creating Si–OH and Si–O–Si bonds, as well as the oxidation of Si–$CH_3$ group by generating Si–O–C and C=O bonds [9, 17–19].

After pyrolysis in the range of 400 to 600°C (Fig. 2c–e), the PCS fibers all showed the main peaks similar to those for the as-cured fiber, implying their organic structure. But differences can be easily recognized in that the Si–H, C–H and Si–$CH_3$ bonds decreased with increase of temperature, especially the Si–H bond,

TABLE III Wavenumbers and assignments of the IR spectrum of PCS

| Wave number ($cm^{-1}$) | Mode of vibration |
|---|---|
| 850–700 | Si—$CH_3$ bending |
| | Si—C stretching in $SiC_4$ |
| 950–800 | Si—H bending |
| 1020 | $CH_2$ bending in Si—$CH_2$—Si |
| 1100–1000 | Si—O stretching in Si—O—Si or Si—O—C |
| 1250 | Si—$CH_3$ stretching |
| 1450–1350 | H stretching in CH, $CH_2$, & $CH_3$ |
| 1720 | C═O stretching |
| 2100 | Si—H stretching |
| 2950–2900 | C—H stretching |
| 3700–3200 | O—H stretching in Si—OH |

which almost disappeared in Fig. 2e for a 600°C-pyrolyzed fiber. In this range, the evolution of low molecular weight molecules and decomposition of organic side groups occurs [16, 20]. Large weight losses and gaseous evolution of mainly $H_2$ and $CH_4$ are associated with these reactions. Si—H and C—H bonds are readily broken [16–18].

When the temperature rises to 700°C (Fig. 2f) or 800°C (Fig. 2g), a new peak assigned to C═C bond appeared at around 1660 $cm^{-1}$, probably due to the dehydrogenation in —CH—CH— fragments [21]. In addition, the C—H and Si—$CH_3$ peaks became undetectable. By 800°C, the organic to inorganic transition is essentially complete and an amorphous residue is obtained, but residual CH or $CH_2$ units still exist in the amorphous residue [18, 21, 22] and they will decompose with further increase in temperatures. This is confirmed by the spectra for the fibers pyrolyzed at higher temperatures, as shown in Fig. 2h to Fig. 2l, in which the $CH_2$ group in the Si—$CH_2$—Si structure decreased gradually and the Si—O peak became more and more evident.

## 3.3. Weight loss and shrinkage behavior

As shown in Fig. 3, the TGA curve of the air-cured PCS fibers suggests that three important transitions occur in the materials as a function of heat treatment temperature, i.e., from 400 to 600°C, 600 to 900°C and 900 to 1250°C. The first stage results in a weight loss

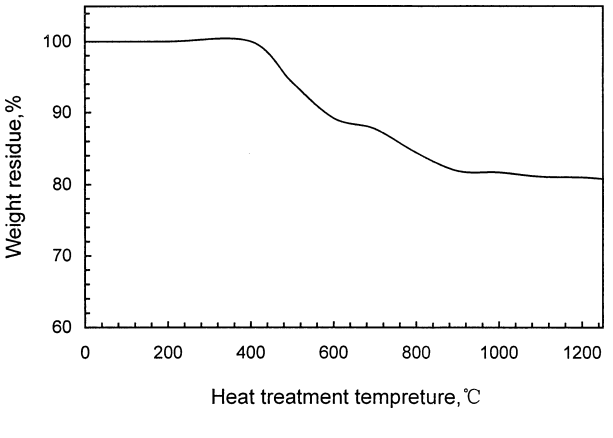


*Figure 3* TGA curve of the air-cured PCS fibers with a heating rate of 100°C/h.

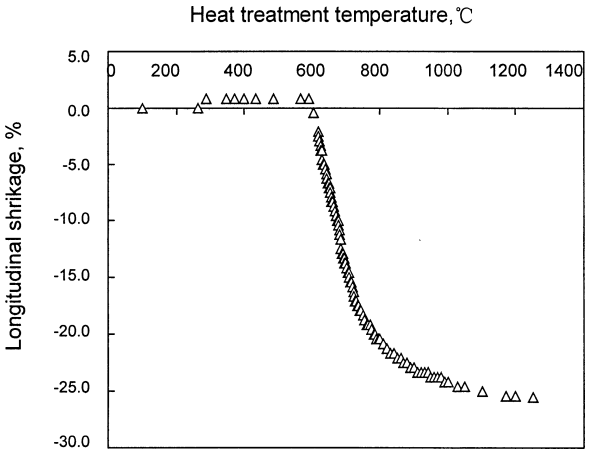


*Figure 4* Longitudinal shrinkage of the air-cured PCS fibers as a function of heat treatment temperature with a heating rate of 100°C/h.

of 10% and is mainly related to evolution of the low molecular weight PCS (LMW-PCS), as well as some gaseous hydrogen and methane due to the breaking of Si—H and C—H bonds, as already inferred from FT-IR analysis. While in the second stage, a critical organic to inorganic transition stage corresponds to the breaking of most organic bonds with the formation of gaseous species. With a weight loss of about 8%, hydrogen and methane are mainly generated in this range [16–18]. After the 900°C-pyrolysis, an amorphous covalent ceramic is obtained with some residual hydrogen (H/Si = ∼0.65) contained in CH groups and the residual hydrogen is responsible for the weight loss of the third stage [23].

Longitudinal shrinkage of a PCS bundle with 200 filaments, as illustrated in Fig. 4, was recorded separately with a load cell of 5g. It can be divided into four stages, therefore, an expanding stage (∼280–600°C), a fast-shrinking stage (600–800°C, −10% per 100°C), a slow-shrinking stage (800–1000°C, −2% per 100°C) and a plane stage (1000–1250°C). Compared with the TG result at the first stage, we can see that not shrinking but expanding occurred although accompanied with a weight loss up to 10 wt%. In addition, the onset temperature of expanding is 100°C lower than that of the weight loss. This is because the material is still in an organic state and its expansion behavior is somewhat related to the structure and the load weight. A large shrinkage occurred from 600 to 800°C. This stage corresponds to the organic to inorganic transition stage with a large density increase from 1.22 to 2.01 $g/cm^3$ (Table II). Therefore, even though a slight weight loss was recorded from 600 to 700°C, microflaws did initiate; moreover, after 800°C, microflaws propagated to the extent that the largest flaw size approached 1.0 $\mu$m. The fibers shrank slowly from 800°C to 1000°C, which also corresponds to a slow weight loss in the TGA curve. After 1000°C, the weight loss reaches a plateau, so does the longitudinal shrinkage.

## 4. Discussion and conclusion

As observed through SEM, microflaws could not be detected below 600°C; they initiated at temperature over

600°C, were visible at ∼700°C and propagated from 700 to 900°C, during which an orientation was shown. Up to 1100°C or 1250°C, the microflaws became interconnected, exhibiting a network morphology. The initiation and propagation of the interior microflaws are closely related to the evolution of gaseous products from the air-cured PCS precursor, which involves a number of stages as characterized above. For discussion purpose, the conversion process was divided into the following stages.

### 4.1. No detectable microflaws (from RT to 600°C)

The important phenomenon that occurs within this temperature range is the evolution of heavy gaseous products corresponding to degradation of polymers of low molecular weight, which results in a large weight loss as established from the TGA result. The organic nature of the PCS precursor does not change markedly as evinced from FT-IR analysis, due to which shrinkage as opposed to expansion occurs within this range. In addition, as already reported elsewhere [22], the reticulation degree increases with increase of temperature due to (1) the condensation of Si─H and Si─$CH_3$ bonds, (2) the oxidation of Si─H bond with absorbed water present in PCS, and (3) the condensation of the Si─OH bond. As a result, both the increased reticulation degree and the expanding property should give a more dense structure instead of a porose one to initiate microflaws. Therefore, no microflaws were formed below 600°C.

### 4.2. Initiation of microflaws (from 600 to 700°C)

This stage originates at the early part of the organometallic-mineral transition stage (∼600 to 800°C), during which most of the Si─H and C─H bonds are broken. Density changes remarkably within this range and significant shrinkage occurs as well. 700°C is a special point in the transition stage not only because interior microflaws come into being but also because nanochannels are formed as well [7–9]. The high content of absorbed water in FT-IR spectrum is an evidence of such a result. The initiations of microflaws and nanochannels are both due to the evolution of gases and of structural changes, but a difference is possible in that microflaws may be avoided if the shrinkage is large enough while nanochannels, as the main channel of evolution of gases, can not be theoretically avoided.

### 4.3. Propagation of microflaws along the "core-edge" direction (from 700 to 1000°C)

Within this range, the microflaws propagated along the "core-edge" direction, especially from 700 to 800°C that locates at the later part of the organic-inorganic transition stage. The reason is similar to that of the initiation of microflaws with the difference that the inorganic property is much increased, as can be inferred from the changes in hydrogen content and density (from 3.09 wt% down to 0.33 wt% and 1.55 g/$cm^3$ up to 2.34 g/$cm^3$, respectively, as shown in Table II). Therefore, difficulties in shrinkage, especially in the transverse direction, are much increased due to the increased stiffness of the material and as a result, the microflaws propagated along the "core-edge" direction.

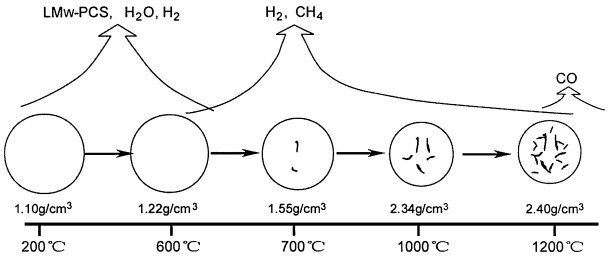


*Figure 5* Illustration for the initiation and propagation behaviors of interior microflaws in the pyrolysis of an air-cured polycarbosilane precursor fiber.

### 4.4. Propagation of microflaws into a network form (from 1000 to 1250°C)

Above 1000°C, weight loss, density and shrinkage all come to a plateau during which residual hydrogen become the main evolution gas, as can be inferred from the FT-IR and chemical compositions. Of course, some trace of CO may also be generated as a result of the decomposition of the silicon oxycarbide phase when the temperature was above 1200°C [16–20]. The 1000°C-pyrolyzed fiber can be essentially regarded as an inorganic material [22] and hence, to some extent, the shrinkage occurs in use of the viscous flow property within this range, as already deduced from SAXS analysis for nanopores which increased in average size but decreased in volume fraction as the temperature increases [8]. As far as the network morphology is concerned, the evolution of hydrogen should be the main factor—short-range order increased and new microflaws initiated across the oriented ones, which then exhibited a network form.

Overall, the initiation and propagation behaviors of the interior microflaws can be illustrated as Fig. 5, in which the evolution of gaseous species, density changes and cross-section morphologies are all shown with increase of heat treatment temperature. That is, the initiation and propagation behaviors of the interior microflaws are closely related to the evolution of the air-cured PCS precursor fibers, during which weight loss, density change and volume shrinkage are considered as the main factors in balancing the volume fraction of porosities (including microflaws and nanopores). If either or both of the weight residue and volume shrinkage are further controlled, the interior microflaws may be somewhat reduced. Further effort is still ongoing.

## References

1. S. YAJIMA, J. HAYASHI and M. OMORI, *Chem. Lett.* **9** (1975) 931.
2. K. J. WYNNE and R. W. RICE, *Ann. Rev. Mater. Sci.* **14** (1984) 297.

3. T. ISHIKAWA, Y. KOHTOKU, K. KUMAGAWA, T. YAMAMURA and T. NAGASAWA, *Nature* **391** (1998) 773.
4. P. BALDUS, M. JANSEN and D. SPORN, *Science* **285** (1999) 699.
5. E. KROKE, Y.-L. LI, C. KONETSCHNY, E. LECOMTE, C. FASEL and R. RIEDEL, *Mater. Sci. Eng.* **R26** (2000) 97.
6. F. CAO, X. D. LI, P. PENG, C. X. FENG, J. WANG and D. P. KIM, *J. Mater. Chem.* **12** (2002) 606.
7. J. LIPOWITZ, H. A. FREEMAN, R. T. CHEN and N. LANGLEY, *Adv. Ceram. Mater.* **2** (1987) 121.
8. J. LIPOWITZ, J. A. RABE, L. K. FREVEL and R. L. MILLER, *J. Mater. Sci.* **25** (1990) 2118.
9. K. SUZUYA, T. KAMIYAMA, T. YAMAMURA, K. OKAMURA and K. SUZUKI, *J. Non-Cryst. Solids* **150** (1992) 167.
10. K. SUZUKI, K. KUMAGAWA, T. KAMIYAMA and M. SHIBUYA, *J. Mater. Sci.* **37** (2002) 949.
11. S. YAJIMA, J. HAYASHI, M. OMORI and K. OKAMURA, *Nature* **261** (1976) 683.
12. Z. Y. CHU, Y. C. SONG, C. X. FENG, Y. S. XU and Y. B. FU, *J. Mater. Sci. Lett.* **20** (2001) 585.
13. Z. Y. CHU, Y. C. SONG, Y. S. XU and Y. B. FU, *ibid.* **18** (1999) 1793.
14. Z. Y. CHU, Y. D. WANG, C. X. FENG, Y. C. SONG, J. WANG, J. Y. XIAO and X. D. LI, *Key Eng. Mater.* **224–226** (2002) 651.
15. Z. Y. CHU, C. X. FENG, Y. C. SONG, Y. D. WANG, X. D. LI and J. Y. XIAO, *T. Nonferr. Metal. Soc.* **12** (2002) 894.
16. Y. HASEGAWA and K. OKAMURA, *J. Mater. Sci.* **21** (1986) 321.
17. H. Q. LY, R. R. TAYLOR, R. J. DAY and F. HEATLEY, *ibid.* **36** (2001) 4037.
18. *Idem.*, *ibid.* **36** (2001) 4045.
19. G. CHOLLON, M. CZERNIAK, R. PAILLER, X. BOURRAT, R. NASLAIN, J. P. PILLOT and R. CANNET, *ibid.* **32** (1997) 893.
20. Y. HASEGAWA and K. OKAMURA, *J. Mater. Sci.* **18** (1983) 3633.
21. G. SORARU, F. BABONNEAU and J. D. MACKENZIE, *J. Non-Cryst. Solids.* **106** (1988) 256.
22. E. BOUILLON, F. LANGLAIS, R. PAILLER, R. NASLAIN, F. CRUEGE, P. V. HUONG, J. C. SARTHOU, A. DELPUECH, C. LAFFON, P. LAGARDE, M. MONTHIOUX and A. OBERLIN, *J. Mater. Sci.* **26** (1991) 1333.
23. G. SORARU, F. BABONNEAU and J. D. MACKENZIE, *ibid.* **25** (1990) 3886.

*Received 12 December 2002*
*and accepted 3 December 2003*